



Mineralization of soil organic matter from equatorial giant podzols submitted to drier pedoclimate: A drainage topochronosequence study

Célia R Montes, Patricia Merdy, Wilson T.L. da Silva, Débora Ishida, Adopho J Melfi, Roberta C Santin, Yves Lucas

► To cite this version:

Célia R Montes, Patricia Merdy, Wilson T.L. da Silva, Débora Ishida, Adopho J Melfi, et al.. Mineralization of soil organic matter from equatorial giant podzols submitted to drier pedoclimate: A drainage topochronosequence study. CATENA, 2023, 222, pp.106837. <10.1016/j.catena.2022.106837>. <hal-04017239>

HAL Id: hal-04017239

<https://hal.science/hal-04017239v1>

Submitted on 31 Mar 2024

HAL is a multi-disciplinary open access archive for the deposit and dissemination of scientific research documents, whether they are published or not. The documents may come from teaching and research institutions in France or abroad, or from public or private research centers.

L'archive ouverte pluridisciplinaire **HAL**, est destinée au dépôt et à la diffusion de documents scientifiques de niveau recherche, publiés ou non, émanant des établissements d'enseignement et de recherche français ou étrangers, des laboratoires publics ou privés.



HAL Authorization

1 **Mineralization of soil organic matter from**
2 **equatorial giant podzols submitted to drier**
3 **pedoclimate: a drainage**
4 **topochronosequence study**

5

6 Célia R. Montes^a, Patricia Merdy^b, Wilson T.L. da Silva^c, Débora
7 Ishida^a, Adolpho J. Melfi^a, Roberta C. Santin^d, Yves Lucas^{b*}

8

9 ^a IEE, NUPEGEL, Universidade de São Paulo, São Paulo 05508-
10 010, Brazil

11 ^b Université de Toulon, Aix Marseille Université, CNRS, IM2NP,
12 83041 Toulon CEDEX 9, France

13 ^c Embrapa Instrumentation, São Carlos 13560-970, Brazil.

14 ^d CENA, Universidade de São Paulo, Piracicaba 13400-970,
15 Brazil

16

17 *Corresponding author (lucas@univ-tln.fr)

18

19

20 **Hightlights**

21

22 • Active hydromorphic podzol in the area store around 63 kgC

23 m⁻²

24 • Erosive incision by a river meander resulted in air entry and

25 oxygenation of the Bh

26 • C content in the Bh of a podzol truncated due to meander

27 diminished by 70%

28 • Drier climate would induce C emission from Amazonian
29 podzol Bhs

30

31

32

33 **Abstract**

34

35 Podzol soils are an important carbon pool in the Amazon, due to
36 the high organic matter (OM) content in their topsoil horizons and
37 deep Bh. To quantify the evolution of the stock and the lability of
38 this carbon pool in the hypothesis of the onset of drier climates, we
39 studied a soil toposequence at the end of which the incision of a river
40 meander lowered the water table, as would result from a drier
41 climate, allowing oxidation the Bh horizons. The soil OM was
42 quantified and characterized (physical fractionation, humification
43 indexes, ^{14}C average age) and its lability under oxic conditions was
44 estimated by measuring respiration during a 660-days experiment.
45 Podzol genesis time was calculated by constraining the carbon fluxes
46 using both C stock and ^{14}C average age. The results confirmed that
47 the studied podzols store large amounts of carbon (62.8 kgC m^{-2} on
48 average). They resulted from a long genesis time, probably greater
49 than 30-50 ky. Topsoil OM is very labile with a residence time of
50 about 100 y; Bh OM is highly humified with a high C/N (62.7 on
51 average) related to low respiration rates. The measured respiration
52 rates were used to estimate the C emission that would result from
53 drier climates at $55 \text{ gC m}^{-2} \text{ y}^{-1}$ on average during the first 100 y,
54 which would correspond, by extrapolation, to $8.5 \cdot 10^{12} \text{ gC y}^{-1}$ for all
55 Amazonian podzols.

56

57

58 Keywords: Amazon podzol; Soil organic matter; Humification
59 index; Soil carbon storage and loss; Climate change; Soil formation
60 rate

61

62

63 **1. Introduction**

64

65

66 Equatorial podzols are characterized by upper organic matter
67 (OM)- rich horizons and thick sandy eluviated horizons (E horizons,
68 also called white sands) overlying deep OM-rich horizons called Bh.
69 In these soils, the dissolved organic matter (DOM) produced in the
70 topsoil is transferred at depth, through the E horizons, by the
71 percolating waters (Lucas, 2001). Part of this DOM is directly
72 exported to the river network by the lateral flow of the groundwater
73 perched on the Bh horizons and circulating in the E horizons. The
74 other part enters the Bh horizons where it can be immobilized as soil
75 organic matter (SOM), remobilized in the perched groundwater
76 (Bardy et al., 2011), mineralized by microbial activity or transferred
77 towards deeper horizons and deep groundwater (Lucas et al., 2012).

78 Despite their very low fertility, equatorial podzols are of interest
79 because, on the one hand, they release large amounts of dissolved
80 organic carbon (DOC) in the river sytem (Leenheer, 1980), most of
81 which is transferred to the sea, participating to the storage of carbon
82 on the scale of geological time (Tardy et al., 2009). On the other
83 hand, since most of them are giant podzols compared to podzols of
84 cold regions, i.e. with E or Bh horizon thicknesses that can reach

85 several meters, they store large amounts of carbon in their upper and
86 Bh horizons: hydromorphic podzols can store more than 100 kgC m⁻²
87 in the whole profile and more than 80 kgC m⁻² in the only deep Bh
88 (Montes et al., 2011). These soil systems therefore contribute
89 significantly to the global CO₂ cycle (Marquez et al., 2016, 2017).
90 The dynamics of DOM transfer and SOM accumulation, however,
91 are still poorly understood.

92 Carbon accumulation in deep Bh horizons is due to the acidic and
93 water-saturated conditions found there. It should be noted that in
94 most areas the hydromorphic podzols are not situated in the bottom
95 of valleys but in a plateau position or on slopes, higher than the
96 phreatic base level (Lucas et al., 1987). As the Bhs have low
97 hydraulic conductivity, they support a perched water-table that joins
98 the deep water-table in restricted parts of the landscape. As a result,
99 the upper part of the Bh is always in waterlogged conditions, which
100 prevents the entry of air from the E horizon into the Bh (Ishida et al.,
101 2014), It can be drained if the climate turns drier, allowing
102 oxygenation of the underlying Bh. For the Upper Rio Negro Basin,
103 where most of the Amazonian podzols are found, climate change
104 modelling predictions point to the gradual onset of a drier season
105 centered around October (Gutiérrez et al., 2021; Iturbide et al., 2021).
106 The CMIP6 model predicted a negligible decrease in annual rainfall,
107 but an increase in the number of consecutive dry days. These were on
108 average 15 days during the 1986-2005 reference period; forecasts
109 were 19 and 31 days for SSP2, near-term period (2021-2040) and
110 SSP5, long-term period (2081-2100), respectively. The CORDEX
111 South America model predicted no change for either scenarios; the
112 CORDEX Central America model predicted 28 and 39 days

113 respectively. An increase in the number of consecutive dry days
114 would alter the dynamics of the water tables perched on the Bh,
115 which could temporarily disappear, allowing air to penetrate into
116 OM-rich horizons that are generally waterlogged. This can lead to
117 increased C mineralization through better aeration satisfying the O₂
118 demand of microorganisms. Increased in dry/wet cycles is also likely
119 to have an impact on the mineralization of C: rewetting of the soil
120 after a period of drying has long been known to cause a burst of
121 respiration (Birch, 1958), so that dry/wet cycles can accelerate soil C
122 loss relative to what would be lost under constant conditions (Miller
123 et al. 2005). Tadini et al. (2018) showed significant compositional
124 changes in the humic acid (HA) fractions of Bh SOM throughout the
125 horizon, with four types of organic matter: recalcitrant, humified, and
126 old dating; labile and young dating; humified and young dating; and
127 little humified and old dating. This suggests a different sensitivity of
128 these organic matters to mineralization processes.

129 In such a context, a first objective of the present work was to
130 evaluate the sensibility to mineralization of the OM issued of
131 hydromorphic podzols to predict the kinetics of CO₂ release after
132 oxygenation.

133 Another way to evaluate the evolution of podzolic OM in a
134 context of climate change is to study a chronosequence where the
135 hydromorphic podzols were progressively submitted to a drier
136 pedoclimate. Two types of such chronosequence can be identified:
137 (1) a Bh formed beneath permanent water table then was submitted to
138 alternating dry and wet conditions due to an external change in
139 drainage conditions and (2) podzols were formed under humid
140 climates then subjected to dryer climates. We have identified in the

141 Amazon a topochronosequence of the first type, for which the change
142 in drainage conditions was a lowering of the water table caused by
143 the erosive incision of a river. The second objective of the present
144 study was therefore to compare the rates of Bh mineralization along
145 this topochronosequence.

146

147

148 **2. Material and methods**

149

150 *2.1. Study area and sampling*

151

152 The study area is situated in Brazilian Amazonia, north of the city
153 of Barcelos, at the edge of the Demini River at the central
154 coordinates 0°17'30"N and 62°48'0"W (Fig. 1). Landscape is a flat
155 area whose altitude is 3 to 15 m over the Demini River higher level.
156 Annual rainfall is around 2600 mm (Reboita et al., 2010) without a
157 marked dry season. The geological substratum, previously considered
158 as a part of the Içá sedimentary formation (Reis et al., 2006), was
159 more recently reclassified as late Pleistocene (129 to 11.7 ky BP) Rio
160 Negro – Rio Branco sedimentary formation, that mainly consists in
161 unconsolidated sands with some clay-silt and conglomerate layers
162 (IBGE, 2011). These sediments were deposited as a megafan
163 following the slow subsidence of the Guyana Shield, giving the
164 largest wetland area of the Amazon (Cremon et al., 2012). After these
165 authors, the studied soils are located on one of the oldest deposit of
166 the megafan whose age, however, is not precisely known. Soils in the
167 area are mainly typical tropical podzols and hydromorphic podzols

168 (Lucas et al., 1996; Dubroeuq and Volkoff, 1998; Montes et al.,
169 2011) associated to some ferralsols which can occur occasionally on
170 scattered hills 2 to 10 m higher than the flat, hydromorphic podzolic
171 inter-hill surface (Pereira et al., 2015). The forest on well-drained
172 podzols is a forest of tall trees, but with low species diversity
173 (Adeney et al., 2016; García-Villacorta et al., 2016); over the
174 hydromorphic podzols is a specific vegetation named campinarana,
175 characterized by a high density of smaller trees (20 to 30 m) that are
176 adapted to physiological stress caused either by waterlogging when
177 the water table is near the surface, or by drought when the water table
178 is further from the surface (Anderson, 1981). In the lowest areas
179 which are always waterlogged, hydromorphic podzols are observed
180 under an herbaceous vegetation forming clumps 20-30 cm high, with
181 the presence of bare patches of white sand.

182 The study area was chosen on the convex side of a meander of the
183 Demini River (Fig. 1), out of the meandering channel in an area
184 where erosion cut directly in the Rio Negro – Rio Branco
185 sedimentary formation, in order to observe the podzol evolution after
186 the lowering of the water table related to the river incision.

187 Soils were studied and sampled by the mean of hand-auger
188 drilling, using casing in the E horizons to avoid sand collapsing in the
189 borehole. Samples for microbial respiration measurements were
190 maintained in the dark at temperature below 5° until analyzed, which
191 occurred within 2 weeks, such a procedure was shown not to affect
192 respiration measurements (Lucas et al., 2020). Samples for soil
193 organic matter (SOM) characterization were frozen and maintained
194 frozen until analyzed. Undisturbed samples for bulk dry density were

195 taken in boreholes by hammering a cylindrical Ø 3 cm piston
196 sampler.

197

198

199 2.2. Laboratory characterizations

200

201 2.2.1. Soil characterization

202 Soil particle size distribution was performed using the Robinson
203 pipette method. Total organic carbon (TOC) was determined using a
204 LECO CR-412 TOC analyser. No carbonates minerals were found in
205 these very acid soils (pH<5) so that in the following "C content" refer
206 to "organic C content". A SOM humification index (H_{LIF}) was
207 obtained by Laser Induced Fluorescence Spectroscopy (LIFS) after
208 Milori et al. (2006): the bulk sample grinded to pass a 250-µm mesh
209 was pressed in pellets and the fluorescence emission spectra between
210 420 and 800 nm under a 405 nm excitation was obtained using a
211 Hamamatsu photomultiplier. The H_{LIF} index was calculated dividing
212 the area of the LIF spectrum by the C content of the sample.

213 The HA fractions were isolated and characterized in a previous
214 work (Tadini et al., 2018) using the procedure recommended by the
215 International Humic Substances Society (Swift, 1996). Here we used
216 the humification index (A_{465}) of HA determined as the total area
217 under the fluorescence emission spectrum recorded at the excitation
218 wavelength of 465 nm (Milori et al., 2002).

219 All mineralogical determinations were performed after organic
220 matter removing with H_2O_2 . Main minerals were identified by XRD
221 (X-ray diffraction) of Cu K α radiation on powder samples using a
222 Philips PW 1877 diffractometer. Kaolinite and gibbsite were

223 confirmed by FTIR (Fourier-transformed Infra-Red spectrometry) on
224 sample-KBr pellets using a Shimadzu IR Prestige-21 spectrometer.
225 Differential thermal analysis (DTA) and thermogravimetric analysis
226 (TGA) were undertaken with a DTG-60H-Simultaneous DTA-TG
227 (Shimadzu, Kyoto, Japan). Goethite was identified using the 488 and
228 413 nm absorption bands (Scheinost et al., 1998) by DRS (Diffuse
229 Reflectance Spectroscopy, Varian Cary 5 spectrometer)

230 Saturated hydraulic conductivity (K_{sat}) was measured on
231 undisturbed samples taken with a Ø 37 mm piston sampler
232 hammered in boreholes. Samples were sealed in a polycarbonate
233 tube, led to water saturation by a 24-h progressive rise of water level
234 from the base of the cylinder, then remained 48 hours for dissolution
235 of the air possibly trapped in the porosity. The water used was
236 previously brought to pH 4 (Lucas et al., 2012) with H_2SO_4 to avoid
237 any dispersion of the organic matter likely to modify the value of
238 K_{sat} .

239 Physical fractionation of the organic matter was realized in
240 triplicate using the procedure described in Sohi et al. (2001). Five
241 grams of soil sieved at 2 mm were placed in centrifuge bottles
242 containing 35 mL of 1.8 g cm^{-3} NaIO_3 solution, manually stirred
243 during 30s then centrifugated at 8000 g during 30 mn. The floating
244 particles, that corresponded to the light free fraction (LFF), were
245 separated by filtration on a GF/A $1.6 \mu\text{m}$ filter. The filtrate was
246 returned to the corresponding centrifuge bottle containing the soil
247 residue and sonicated. Floating particles corresponded to a light intra-
248 aggregate fraction, the light occluded fraction (LOF), they were
249 separated by centrifugation and filtration as for LFF. The OM
250 remaining in the centrifugation pellet corresponded to the heavy

251 fraction (HF). C on the filters and on the final centrifugation pellets
252 was quantified as for TOC.

253

254 2.2.2. *Basal respiration*

255 Soil respiration was determined using the method described in
256 Paul et al. (2001). The respiration gas samples were analyzed for CO₂
257 concentrations using a GC-17A Shimadzu gas chromatograph
258 equipped with a flame ionization detector. After extraction, jars were
259 opened for 5 mn for equilibrating with external atmosphere.
260 Sampling was done twice a week during the 2 first weeks, then thrice
261 a week until 3 months, then weekly until 4 months, then monthly
262 until the end of experiment that was stopped after 660 days. Detailed
263 data are given in supplementary material; they were used to calculate
264 the cumulative respiration during the 660 days long experiment and
265 the SOM respiration rates using a 2 pools model, each pool having a
266 first order kinetics. The respiration curves were fitted by the Excel
267 Solver using the Evolutionary algorithm to find the parameters values
268 that minimized the normalized root mean square deviation (RMSD).
269 Examples of respiration curves and processing are given in Lucas et
270 al. (2020).

271

272 2.2.3. *Isotopic measurements*

273 After freeze drying, soil samples were ground to pass a 106-μm
274 mesh. Between 35 to 90 mg of the sample, depending on carbon
275 concentration, was transferred to a tin capsule for elemental and
276 isotopic analysis. The isotope ratios of carbon (¹³C/¹²C) and nitrogen
277 (¹⁵N/¹⁴N) of each sample were determined using a continuous-flow
278 isotope ratio mass spectrometer (Delta Plus, ThermoFisher Scientific,

279 Bremen, Germany) coupled to an elemental analyzer (CHN-1110,
280 Carlo Erba, Rodano, Italy). Carbon and nitrogen isotope
281 compositions were calculated as:

282

$$283 \quad \delta (\text{‰}) = [(R_{\text{sample}}/R_{\text{standard}}) - 1] \times 1000$$

284

285 where R is the ratio of $^{13}\text{C}/^{12}\text{C}$ or $^{15}\text{N}/^{14}\text{N}$. Stable isotope ratios for
286 C were measured using internationally standard PDB (Limestone
287 from the Grand Canyon region, USA) while the standard for nitrogen
288 was atmospheric air.

289

290 *2.2.4. Radiocarbon measurement*

291 Radiocarbon measurements were carried out at the Poznań
292 Radiocarbon Laboratory, Poland. Radiocarbon dating of organic
293 matter must be corrected for "bomb carbon", the atmospheric ^{14}C
294 peak brought by the tropospheric nuclear tests of the 1960s
295 (Trumbore, 2000). In the Bh, we assumed that the proportion of
296 bomb carbon in the Bh organic matter was negligible and we
297 calculated a conventional, uncalibrated age from the radiocarbon
298 pMC (percent modern carbon) value. This age is an apparent age
299 because the Bh are open systems mixing organic carbon of different
300 ages. The topsoil organic matter, however, was very younger and had
301 a significant amount of post-bomb carbon, giving a pMC higher than
302 100 %. In such case, we assumed that the topsoil horizons reached a
303 steady state before 1950 and calculated an apparent age using the
304 method given in Doupoux et al. (2017).

305

306

307 2.3. *Statistical analysis and modelling*

308 Statistical analysis was performed using XLSTAT2017. We chose
309 a correlation-type PCA on standardized variables to avoid sensitivity
310 to the scaling of the variables. Modelling was realized using the
311 method developed in Doupoux et al. (2017), in which the podzol
312 profile genesis time is constrained by both total carbon and
313 radiocarbon. For a given C pool, assuming a constant input of C and
314 a constant rate for C outflow, the relationships between total carbon
315 and radiocarbon can be calculated analytically. This allows the
316 calculation of the minimum time required to form the carbon pool.
317 The authors applied this method to give an estimate of the minimum
318 time required to form a given profile by considering three carbon
319 pools: a topsoil C pool and two pools in the Bh: a fast Bh pool (high
320 C turn-over) and a slow Bh pool (low turn-over).

321 The model required knowing the radiocarbon and total carbon
322 values in each pool. Total carbon was calculated from carbon weight
323 % and bulk density. Radiocarbon and carbon % were measured; the
324 bulk density was measured for some samples and, for the others,
325 estimated using the following equation proposed by Pereira et al.
326 (2016):

327

$$\begin{aligned} \rho_p = & 1.463 + 0.1998 \tan[1.044 - 0.002 (\text{clay})] \cos[0.125 + \\ & 0.135(C/N) + (3.543 \cdot 10^{-5}) (\text{silt})^2 - 0.013 (\text{silt})] \cos[0.004 (\text{fine sand}) \\ & \cos(0.315 + \tan[0.005 (\text{clay}) - 2.317]) - 1.065 \cos[0.315 + \tan(0.005 \\ & (\text{clay}) - 2.317))] - 0.144 (\text{total } N) \end{aligned}$$

332

333 where *clay*, *silt*, *fine sand*, *C*, *N* and *total N* are expressed in g kg⁻¹
334 ¹. Total carbon stock as well as apparent ¹⁴C age was calculated
335 using linear interpolation between sampled depth.

336

337

338 **3. Results and discussion**

339

340 *3.1. Soils description and main characteristics*

341

342 The soils presented and discussed here (BAR1 to BAR6) are
343 located in Fig. 1. The BAR1, BAR2 and BAR4 soil are situated on a
344 toposequence (Fig. 2) starting from a waterlogged zone, in which the
345 water table is all the time near or above the soil surface, until at the
346 bank of the Demini River. BAR3 is in a position equivalent to that of
347 BAR2 (Fig. 1), but in a more hydromorphic zone characterized by
348 Campinarana-type forest and "murundus" micro-relief, i.e. earth
349 mounds, about 0.6 m high and 2-10 m wide, separated by U-shaped
350 channels, as described in Ishida et al. (2014). Soils BAR5 and 6 are
351 located further towards the centre of the highly hydromorphic area,
352 which is waterlogged most of the year (Fig. 1). BAR1 to BAR4 soils
353 have been studied analytically in detail; all laboratory analysis are
354 given in Supplementary material (Tab. S1).

355 All the soils were sand to loamy sand over the whole profile,
356 except BAR1 mainly sandy loam, and BAR3, sandy loam in the
357 upper part of Bh (Fig. 3). In all soils, apart from a few heavy
358 minerals as zircon and ilmenites, the identifiable minerals were
359 quartz, kaolinite, gibbsite and goethite (Fig. 4). In all E horizons,

360 quartz was the only mineral observed. Kaolinite was observed in
361 trace amounts ($<0.5\%$) in other horizons and in quantifiable amounts
362 at depth. Goethite and gibbsite were observed at depth in BAR1 and
363 along the whole profile in BAR4.

364 The upper soil horizons varied according to local waterlogging
365 conditions. In the mostly waterlogged areas (BAR1, BAR3, BAR5
366 and BAR6), the surface horizon was a sticky, very fine-grained black
367 peat (P horizons). In better drained areas, it was an A horizon. E
368 horizons were well expressed and light in color (grey to light grey)
369 except for BAR1, where it was weakly expressed, and BAR4, where
370 it was absent. In the Bh horizons the C content ranged between 0.25
371 and 3.28 % (average 1.09%), unrelated with soil colour darkness
372 (hue) (Munsell, 1990). The C content varied with depth but was
373 higher in the upper indurated part of BAR2 and BAR3 Bhs.
374 Considering all Bhs together, there was surprisingly no correlation
375 between C content and clay, silt, (clay + silt) or kaolinite content (R^2
376 values < 0.13), while several studies point to the role of absorption
377 on clay and oxide surfaces in immobilization of DOM (Kaiser and
378 Zech, 2000; Merdy et al., 2021). Considering the soils separately,
379 however, a correlation was observed between C content and clay
380 content for BAR2 and BAR3 soil (R^2 equal to 0.56 and 0.50,
381 respectively) and between C content and silt content in the BAR1 soil
382 (R^2 equal to 0.39), which indicates that in these sandy materials the
383 SOM tends to accumulate at the finest grain size levels.

384 A perched water table was observed above the Bh in the BAR2
385 and BAR3 soils. The saturated hydraulic conductivity K_{sat} was
386 determined on three samples from the upper part of the BAR3 Bh (at
387 165-170 cm depth for each sample). The results gave a very low

388 average value ($7.7 \cdot 10^{-9} \pm 2.3 \cdot 10^{-9} \text{ m s}^{-1}$), which corresponds to an
389 impervious material, in accordance with the presence of perched
390 groundwater. A hydrogen sulfide odor, indicating reducing
391 conditions, was detected during drilling of the Bh horizons of all
392 profiles except BAR4.

393 BAR2 and BAR3 soils are typical giant equatorial podzols, with a
394 bleached sandy E horizon more than 1 m thick overlying a thick Bh.
395 In areas that are mostly waterlogged, podzols profiles are either
396 thinner (BAR5 and BAR6 soils) or less developed, such as BAR1
397 soil where the E horizon is not bleached, probably because the lateral
398 throughflow of the perched groundwater is slower. In the BAR4
399 profile, the E horizons and the indurated upper part of the Bh have
400 been removed by erosion due to the meanders of the Demini river.
401 The % carbon in the topsoil horizon as well as in the Bh are
402 significantly lower than in the BAR2 and BAR3 profile, indicating
403 that profile truncation likely resulted in a loss of carbon throughout
404 the profile. It should be noticed that the horizon situated beneath the
405 Bh was not reached for the BAR2 and BAR3 profiles despite the
406 casing of the borehole: the groundwater sapping in depth resulted in
407 the rise in the borehole of a mixture of groundwater and Bh material.

408

409

410 *3.2. Soil organic matter*

411

412 *3.2.1. Fractionation and humification indexes*

413 The results of the organic matter fractionation of the BAR1,
414 BAR3 and BAR4 soils are given in Fig. 5. Uncomplexed OM (LFF
415 and LOF fractions) is usually considered as a transient pool between

undecomposed litter and mineral-associated OM (HF fraction), with the turnover of LFF and HF respectively being the faster and the lower (Christensen, 2001). Here the highest LFF percentages were observed in the topsoil horizons and decreased in the top 50 cm while the LOF and HF percentages increased, indicating progressively stronger bonds with mineral material, although it was very sandy. In these horizons, a strong negative correlation was observed between LFF and LOF (Fig. 6), suggesting that LFF transformed into LOF with depth. In BAR1 and BAR3 Bhs, the HF percentage in SOM increased rapidly with depth, up to more than 70% around 2 m in depth, then gradually decreased. The positive correlation between LFF and LOF in BAR1 suggests that these fractions were both transformed to HF in the upper 2 m of Bh, and both produced from HF or brought by percolating solutions or deep groundwater to the transition towards the C horizon. A part of the highly humified OM can however appear in the LFF fraction (Cadisch et al., 1996). In BAR4 Bh, the SOM fractions are from 50 cm depth similar to those observed at depth in BAR3 Bh, which is consistent with the hypothesis of a truncated soil.

There was no significant correlation between the humification index A_{465} (Tadini et al., 2018) and any of the LFF, LOF and HF fractions, indicating that aromaticity was not related to a specific fraction. The A_{465} index was however higher in the BAR4 soil than in other soils, which indicates that since the lowering of the water table, the less aromatic compounds have been preferentially leached or mineralized.

Considering all the samples, there was no correlation between the H_{LIFS} index and the A_{465} index (Table 1). As pointed out by Tadini et

al. (2018), this is probably due to fluorescence self-absorption of dark Bh samples and these authors proposed a colour-corrected index (H_{LIFS-M}) calculated by dividing the H_{LIFS} index by the Munsell colour value of the bulk sample. The correlation, however, was also very weak between the colour-corrected index H_{LIFS-M} and the A_{465} index (Table 1). By gradually restricting the sample population to samples belonging to narrower colour range, the correlations between H_{LIFS} and H_{LIFS-M} indexes and the A_{465} index become progressively higher: R^2 between H_{LIFS-M} and A_{465} was 0.79 when considering only samples with a colour value <4 . This indicates that the H_{LIFS} signal is indeed dependent on the degree of humification, but that the colour interference masks this dependence: black material lowered the fluorescence signal by absorption when white material exhausted the fluorescence signal by diffusion. The correction proposed by Tadini et al. (2018) was insufficient for our sample set. Pending the development of an effective correction, it is therefore advisable to restrict the use of the H_{LIFS} or H_{LIFS-M} indexes to samples belonging to a restricted colour range.

462

463 **Table 1**

464 Pearson coefficient of determination R^2 between A_{465} index and H_{LIFS} ,
465 H_{LIFS-M} indexes

466

	H_{LIFS}	H_{LIFS-M}
All samples (n = 20)	0.06	0.12
Samples with colour value <5 (n = 13)	0.47	0.73
Samples with colour value <4 (n = 11)	0.65	0.79

467

468

469 *3.2.2. Apparent age, C/N, respiration and isotopic data*

470 The SOM of all topsoil horizons had a low apparent ^{14}C age (<110
471 y), indicating an average C turnover around 100 y (Trumbore, 2000),
472 and a C/N < 25 (Fig. 7). Cumulative respiration was very high for the
473 more hydromorphic P horizons (BAR1 and BAR3). In the well-
474 expressed E horizons (BAR2 and BAR3), ages ranged from 205 to
475 830 y, C/N from 32 to 37 and cumulative respiration was high. In the
476 Bh horizons, the apparent ages were variable but all high, ranging
477 from 2510 to 9980 y. The C/N was higher than 40 (62,7 cm on
478 average) in all the Bhs of untruncated podzols, that is to say profiles
479 BAR1, -2, -3 where the water table have not been lowered. In BAR4,
480 it ranged from 21 to 31. There were no significant differences
481 between the profiles for $\delta^{13}\text{C}$, which increased slightly with depth,
482 whereas the values of $\delta^{15}\text{N}$ were more discriminating with higher
483 values for the BAR4 whole profile and the BAR2 topsoil (Fig. 8).

484 A principal component analysis (PCA) was performed on all
485 the parameters discussed above, to which were added the values of
486 the N % in the SOM humic acid fractions (%N HA, data from Tadini
487 et al., 2018) (Fig. 9). It showed a positive Pearson correlation ($R >$
488 0.65) between ^{14}C age, A_{465} index, depth, $\delta^{13}\text{C}$ on one side and
489 between N(%), %N HA on the other, the variables from one group
490 having negative correlations ($R < -0.65$) with those from the other
491 group. It also showed a very negative correlation between $\delta^{15}\text{N}$ and
492 C/N.

493 These relationships indicate that, on the one hand, the increase in
494 age is related to the increase in aromaticity and $\delta^{13}\text{C}$ and the decrease
495 in N%, especially in HA, which is the expected SOM evolution in the
496 Bh, resulting in a C/N greater than 45. In the BAR4 profile and the

497 BAR2 topsoil, the lower C/N and higher $\delta^{15}\text{N}$ indicate that the
498 lowering of the water table has resulted in a better oxygenation and N
499 supply from the topsoil, promoting microbial activity which
500 consumed C and increased ^{15}N (Kamer et al., 2003; Dijkstra et al.,
501 2006).

502

503 3.2.3. *Respiration kinetics*

504 Results of the modelling of the respiration data are given in Fig.
505 10. Topsoil horizons were characterized by a fast pool having a larger
506 relative size when hydromorphic (BAR3), and smaller when better
507 drained (BAR2 and BAR4). Well expressed E horizons (BAR2 and
508 BAR3) showed a large relative size of the fast pool and high
509 respiration rates in fast and slow pools. Bh horizons showed a low
510 relative size of the fast pool and low respiration rates of the slow
511 pool, consistent with high aromaticity and high C/N. In the BAR4
512 profile these latter characteristics were observed up to the topsoil,
513 indicating that over the entire profile the slow pool has not, or very
514 little, rejuvenated after truncation.

515 The respiration rates obtained here can be compared to respiration
516 rates obtained for other soils with similar methods at a temperature
517 comprised between 25 and 30° (Fig. 11). Yang et al. (2007), Haddix
518 et al. (2011) and Kern et al. (2019) provided data from topsoil
519 horizons of a variety of soil types from cold to hot, and humid to dry
520 climates; Lucas et al. (2020) provided data from topsoil and Bh
521 horizons of other Amazonian podzols. The respiration rates obtained
522 here are in the same range that those obtained for the topsoil of other
523 soil types regarding the fast pool, but lower regarding the slow pool.
524 For the latter, the respiration rate were in the range $[2.4 \cdot 10^{-2} - 5.0 \cdot 10^{-2}]$

525 $^1] \text{ y}^{-1}$ for topsoil of other soil types, $[2.4 \cdot 10^{-3} - 1.8 \cdot 10^{-2}] \text{ y}^{-1}$ for topsoil
526 of untruncated podzols and $[6.8 \cdot 10^{-4} - 2.4 \cdot 10^{-3}] \text{ y}^{-1}$ for the Bh
527 horizons. The respiration rate of the Bh slow pool is therefore on
528 average about 2 orders of magnitude lower than that observed for the
529 topsoil of most soils.

530

531 *3.3. Carbon stock and soil genesis*

532

533 *3.3.1. Profile genesis*

534 The untruncated podzol profiles, where the water table has not
535 been lowered, store large amount of C (at least 67.9, 73.7 and 56.8 kg
536 C m^{-2} for profiles BAR1, -2 and -3, respectively). The average is 62.8
537 kg ha^{-1} , which is consistent with the results of previous studies
538 (Montes et al., 2012; Pereira et al., 2016; Doupoux et al., 2017). We
539 calculated the minimum time required to form the presently observed
540 BAR1, BAR2 and BAR3 profiles and the time required to reach 99%
541 of the observed ^{14}C age and Bh C pool, considering that these values
542 correspond to a steady state (Fig. 11 and Table 2). The calculations
543 gave a range of time according to assumptions about the size of the
544 fast Bh pool. The minimum time to form the profile is a lower bound
545 but not likely, because it corresponds to a scenario with no C outflux
546 from the Bh and in which the profile evolves very quickly (Fig. 12).
547 The time needed to reach 99% of the steady state gives a more
548 probable order of magnitude of the minimum genesis time. The
549 BAR4 profile was not considered because, truncated, it does not meet
550 the conditions of constant flux rates with time.

551 The order of magnitude of the time to reach 99% of steady state is
552 around 30000 y for the BAR1 and BAR2 profiles and around 50000

years for the BAR3 profile (Table 2). For the BAR2 and BAR3 profiles these times are certainly underestimated because the horizon located beneath the Bh was not reached during the drilling so that the Bh total C stock and therefore the genesis time were underestimated. Regardless, these results are consistent with the late Pleistocene age of the parent material and show that these podzols accumulated organic carbon for a very long time.

Table 2

Carbon stock, apparent age and time required to form the profiles

Profile	P or A horizons		Bh horizon		Minimum time to form the profile (y)	Time to reach 99% of steady state (y)
	Carbon stock (kg m ⁻²)	Apparent age (y BP)	Carbon stock (kg m ⁻²)	Apparent age (y BP)		
BAR1	29.59	110	35.58	4785	9690 – 11400	29250 – 30380
BAR2	6.71	105	59.95	4689	9830 – 10550	28700 – 29400
BAR3	7.84	108	37.51	6699	14800 – 18260	48640 – 54215
BAR4	3.73	106	19.28			

3.3.2. Soil OM dynamics after truncation

How much and at what rate was the organic carbon of the BAR4 profile mineralized after truncation of the profile and corresponding oxygenation of the Bh? To obtain an order of magnitude, the initial C content of the BAR4 profile can be assumed to be the same as that currently observed in the untruncated podzol, which will be represented here by the average of the BAR2 and BAR3 profiles. Measured respiration rates allow calculation of how long it takes to decrease the C content of untruncated podzol to the BAR4 values and how much C would be released into the atmosphere after the perched groundwater disappears and oxygenated air enters the Bh. The

576 calculation was performed using the following equation, and the data
577 used for the calculation is given in Table 3.

578

579
$$C = C_0 \left(f_{Fp} (e^{-k_{Fp}t}) + (1 - f_{Fp}) (e^{-k_{Sp}t}) \right)$$

580

581 Where C is the carbon pool at time t , C_0 the initial carbon pool, f_{Fp}
582 the initial fast pool fraction, k_{Fp} and k_{Sp} the respiration rate of the fast
583 and the slow pool, respectively. The results are that it takes about 10
584 and 1220 y for topsoil horizon and Bh, respectively, to derive BAR4
585 values from untruncated podzol values. The latter seems consistent
586 with the rate of bank erosion by an Amazonian meander, estimated
587 at, in m y^{-1} , 0.008 to 0.015 of the meander width (Constantine et al.,
588 2014), which would give a displacement of 1 to 2 m y^{-1} for the
589 Demini meander. It should be noted, however, that the lateral
590 widening of the flood plain is slower than the displacement of a
591 meander (Camporeale et al., 2006).

592 Assuming that the disappearance due to climate change of the
593 permanent water-table perched above the Bh would have the same
594 consequence as what was observed in the topochronosequence, we
595 can extrapolate the measured mineralization rate to the Amazonian
596 podzol area. The carbon pools decrease being exponential, the
597 emission of C per year decreases over time: it is on average about 63
598 $\text{gC m}^{-2} \text{y}^{-1}$ during the first 10 years, 54 $\text{gC m}^{-2} \text{y}^{-1}$ during the
599 following 90 years and 41 $\text{gC m}^{-2} \text{y}^{-1}$ during the following 400 years.
600 These values, related to the 155000 km^2 of the Amazonian podzol
601 area (Montes et al., 2011), would correspond to an emission of C into
602 the atmosphere about $9.8 \cdot 10^{12}$, $8.4 \cdot 10^{12}$, $6.3 \cdot 10^{12} \text{ gC y}^{-1}$ for the 0-10 y,

10-100 y, 100-500 y periods, respectively. These values, however, remain low compared to current carbon emission by fossil fuels (about $9 \cdot 10^{15} \text{ g y}^{-1}$, IEA (2020)). It should also be noted that other processes may arise after Bh oxygenation begins. Some can accelerate degradation, such as the addition of nitrogen from the surface horizons (Qiao et al., 2016) or fluctuating water content (Van Gestel et al., 1993), others can slow it down, such as substrate availability (Wei et al., 2015). **Table 3**

Data for calculation of SOM mineralization after truncation.

Untruncated podzol values are the average of values obtained for the BAR2 and BAR3 profiles.

	C content		Fast pool fraction	Respiration rate (y ⁻¹)	
	kg m ⁻²	kg m ⁻³		Fast pool	Slow pool
Topsoil horizons					
Untruncated podzol	7.27	11.88	1.25 10 ⁻³	7.70	1.01 10 ⁻²
BAR4	3.73	10.68	5.04 10 ⁻³	6.96	7.72 10 ⁻⁴
Bh					
Untruncated podzol	48.73	19.43	1.25 10 ⁻³	4.54	1.18 10 ⁻³
BAR4	19.28	4.59	1.22 10 ⁻³	7.08	6.76 10 ⁻⁴

614

615

616 4. Conclusions

617

The studied toponomosequence comprised typical equatorial giant podzol and equatorial hydromorphic podzols, both of which with a perhumid Bh under reducing conditions. They store large amounts of C (62.8 kg m^{-2} on average) and result from a long genesis time the minimum estimate of which is around 10-20 ky, but which is very probably greater than 30-50 ky. The organic matter of topsoil had a rapid average turnover, about 100 y, therefore likely to mineralize very quickly in the event of a change towards a drier

626 climate. In the Bh of these podzols, increased OM age was related to
627 increased heavy fraction, aromaticity, C/N and $\delta^{13}\text{C}$. The H_{LIFS}
628 humification index was found to be inappropriate for these soils, due
629 to interference with the soil colour.

630 The lowering of the water table in part of the topochronosequence
631 and the subsequent oxygenation of the Bh resulted in a decrease in
632 the Bh C stock from about 19 kgC m^{-3} to 5 kgC m^{-3} that requires,
633 according to measured respiration rates, a duration of around 1200 y.

634 Applying these respiration rates to the Bh oxygenation that would
635 result from climate change gives a rough estimate of subsequent C
636 emission, around $55 \text{ gC m}^{-2} \text{ y}^{-1}$ on average during the first 100 years.
637 Extrapolated to all Amazonian podzols, and regardless of other
638 processes that may be involved, this value would correspond to 8.5
639 $10^{12} \text{ gC y}^{-1}$.

640

641

642 **CRedit authorship contribution statement**

643

644 **Célia R. Montes:** Conceptualization, Methodology, Writing -
645 Original Draft, Investigation, Supervision, Project administration,
646 Funding acquisition. **Patricia Merdy:** Methodology, Formal
647 analysis, Writing – review & Editing. **Wilson T.L. da Silva:**
648 Investigation, Supervision. **Débora Ishida:** Investigation,
649 Ressources. **Adolpho J. Melfi:** Investigation, Writing – review &
650 Editing. **Roberta C. Santin:** Investigation. **Yves Lucas:**
651 Conceptualization, Methodology, Data Curation, Writing - Original
652 Draft, Supervision, Project administration, Funding acquisition.

653

654 **Declaration of Competing Interest**

655

656 The authors declare that they have no known competing financial
657 interests or personal relationships that could have appeared to
658 influence the work reported in this paper.

659

660 **Funding**

661

662 This work was supported by the São Paulo Research Foundation
663 (FAPESP) [grants numbers #2011/03250-2; #2012/51469-6, doctoral
664 scholarship #2012/18092-6]; the National Council for Scientific and
665 Technological Development (CNPq) [research scholarship to CRM
666 #303478/2011-0; #306674/2014-9]; and French Agence Nationale de
667 la Recherche (ANR) [grant number ANR-12-IS06-00002 “C-
668 PROFOR”].

669

670

671 **Appendix A. Supplementary data**

672

673

674 **References**

675

676 Adeney, J.M., Christensen, N.L., Vicentini, A., Cohn-Haft, M., 2016.
677 White-sand ecosystems in Amazonia. *Biotropica* 48, 7-23.
678 <https://doi.org/10.1111/btp.12293>.

679 Anderson, A.B., 1981. White-sand vegetation of Brazilian Amazonia.
 680 Biotropica 13, 199–210. <https://doi.org/10.2307/2388125>
 681 Bardy, M., Derenne, S., Allard, T., Benedetti, M. F., Fritsch, E.,
 682 2011. Podzolisation and exportation of organic matter in black
 683 waters of the Rio Negro (upper Amazon basin, Brazil).
 684 Biogeochem. 106, 71–88. <https://doi.org/10.1007/s10533-010->
 685 9564-9
 686 Birch, H.F., 1958. The effect of soil drying on humus decomposition
 687 and nitrogen availability. Plant Soil 10, 9–31.
 688 <https://doi.org/10.1007/BF01343734>
 689 Cadisch, G., Imhof, H., Urquiaga, S., Boddey, R.M., Giller, K.E.,
 690 1996. Carbon turnover ($\delta^{13}\text{C}$) and nitrogen mineralization
 691 potential of particulate light soil organic matter after rainforest
 692 clearing. Soil Biol. Biochem. 28, 1555-1567.
 693 [https://doi.org/10.1016/S0038-0717\(96\)00264-7](https://doi.org/10.1016/S0038-0717(96)00264-7)
 694 Camporeale, C., Perona, P., Porporato, A., Ridolfi, L.U.C.A., 2007.
 695 Hierarchy of models for meandering rivers and related
 696 morphodynamic processes. Rev. Geophys. 45, RG1001.
 697 <https://doi.org/10.1029/2005RG000185>.
 698 Christensen B.T., 2001. Physical fractionation of soil and structural
 699 and functional complexity in organic matter turnover. Eur. J.
 700 Soil Sci. 52, 345-353. <https://doi.org/10.1046/j.1365->
 701 2389.2001.00417.x
 702 Constantine, J.A., Dunne, T., Ahmed, J., Legleiter, C., Lazarus, E.D.,
 703 2014. Sediment supply as a driver of river meandering and
 704 floodplain evolution in the Amazon Basin. Nature Geoscience 7,
 705 899-903. <https://doi.org/10.1038/NGEO2282>

706 Cremon, E.H., Rossetti, D.F. and Zani, H., 2012. Gênese e evolução
707 geomorfológica do megaleque Demini (norte da Amazônia)
708 baseado na análise morfoestrutural e hidroperíodo. Anais 9º
709 SINAGEO, 2012, Rio de Janeiro.
710 <http://www.sinageo.org.br/2012/trabalhos/2/2-440-165.html>
711 (accessed 21 October 2020).

712 Dijkstra, P., Ishizu, A., Doucett, R., Hart, S.C., Schwartz, E.,
713 Meyailo, O.V., Hungate, B.A., 2006. ¹³C and ¹⁵N natural
714 abundance of the soil microbial biomass. Soil Biol. Biochem.
715 38, 3257-3266. <https://doi.org/10.1016/j.soilbio.2006.04.005>

716 Dubroeuq, D., Volkoff, B., 1998. From oxisols to spodosols and
717 histosols: evolution of the soil mantles in the Rio Negro Basin
718 (Amazonia). Catena 32, 245-280. [https://doi.org/10.1016/S0341-](https://doi.org/10.1016/S0341-8162(98)00045-9)
719 [8162\(98\)00045-9](https://doi.org/10.1016/S0341-8162(98)00045-9)

720 Doupoux, C., Merdy, P., Montes, C.R., Nunan, N., Melfi, A.J.,
721 Pereira, O.J.R., Lucas, Y., 2017. Modelling the genesis of
722 equatorial podzols: age and implications for carbon fluxes,
723 Biogeosciences 14, 2429–2440. [https://doi.org/10.5194/bg-14-](https://doi.org/10.5194/bg-14-2429-2017)
724 [2429-2017](https://doi.org/10.5194/bg-14-2429-2017).

725 García-Villacorta, R., Dexter, K.G., Pennington, T., 2016.
726 Amazonian white-sand forests show strong floristic links with
727 surrounding oligotrophic habitats and the Guiana Shield.
728 Biotropica 48, 47-57. <https://doi.org/10.1111/btp.12302>.

729 Gutiérrez, J.M., R.G. Jones, G.T. Narisma, L.M. Alves, M. Amjad,
730 I.V. Gorodetskaya, M. Grose, N.A.B. Klutse, S. Krakovska, J.
731 Li, D. Martínez-Castro, L.O. Mearns, S.H. Mernild, T. Ngo-
732 Duc, B. van den Hurk, and J.-H. Yoon, 2021: Atlas. In Climate
733 Change 2021: The Physical Science Basis. Contribution of

734 Working Group I to the Sixth Assessment Report of the
 735 Intergovernmental Panel on Climate Change [Masson-Delmotte,
 736 V., P. Zhai, A. Pirani, S.L. Connors, C. Péan, S. Berger, N.
 737 Caud, Y. Chen, L. Goldfarb, M.I. Gomis, M. Huang, K. Leitzell,
 738 E. Lonnoy, J.B.R. Matthews, T.K. Maycock, T. Waterfield, O.
 739 Yelekçi, R. Yu, and B. Zhou (eds.)]. Cambridge University
 740 Press. In Press. Interactive Atlas available from Available from
 741 <http://interactive-atlas.ipcc.ch/>
 742 Haddix, M.L., Plante, A.F., Conant, R.T., Six, J., Steinweg, J.M.,
 743 Magrini-Bair, K., Drijber, R.A., Morris, S.J., Paul, E.A., 2011.
 744 The role of soil characteristics on temperature sensitivity of soil
 745 organic matter. *Soil Sci. Soc. Am. J.* 75, 56-68.
 746 <https://doi.org/10.2136/sssaj2010.0118>
 747 IBGE, 2011. Diretoria de Geociências (DGC). Coordenação de
 748 Recursos Naturais e Estudos Ambientais (CREN). Mapas
 749 georeferenciados de recursos naturais. Escala 1: 250:000, formato
 750 digital: shp. Rio de Janeiro, 2008.
 751 [ftp://geoftp.ibge.gov.br/informacoes_ambientais/geologia/levantamento_geologico/mapas/unidades_da_federacao/am_geologia.](ftp://geoftp.ibge.gov.br/informacoes_ambientais/geologia/levantamento_geologico/mapas/unidades_da_federacao/am_geologia.pdf)
 752 [pdf/](ftp://geoftp.ibge.gov.br/informacoes_ambientais/geologia/levantamento_geologico/mapas/unidades_da_federacao/am_geologia.pdf) (accessed 21 October 2020).
 753
 754 IEA, 2020. Global CO2 emissions in 2019, IEA, Paris.
 755 <https://www.iea.org/articles/global-co2-emissions-in-2019/>
 756 (accessed 21 October 2020).
 757 Ishida, D.A., Montes, C.R., Lucas, Y., Pereira, O.J.R., Merdy, P.,
 758 Melfi, A.J., 2014. Genetic relationships between ferralsols,
 759 podzols and white kaolin in Amazonia. *Eur. J. Soil Sci.* 65, 706-
 760 717. <https://doi.org/10.1111/ejss.12167>

761 Iturbide, M., Fernández, J., Gutiérrez, J.M., Bedia, J., Cimadevilla,
 762 E., Díez-Sierra, J., Manzananas, R., Casanueva, A., Baño-Medina,
 763 J., Milovac, J., Herrera, S., Cofiño, A.S., San Martín, D., García-
 764 Díez, M., Hauser, M., Huard, D., Yelekci, Ö., 2021. Repository
 765 supporting the implementation of FAIR principles in the IPCC-
 766 WG1 Atlas. Zenodo, DOI: 10.5281/zenodo.3691645. Available
 767 from: <https://github.com/IPCC-WG1/Atlas>
 768 Kaiser, K., Zech, W., 2000. Dissolved Organic Matter sorption by
 769 mineral constituents of subsoil clay fractions. *J. Plant Nutr. Soil*
 770 *Sci.* 163, 531–535. [https://doi.org/10.1002/1522-](https://doi.org/10.1002/1522-2624(200010)163:5<531::AID-JPLN531>3.3.CO;2-E)
 771 [2624\(200010\)163:5<531::AID-JPLN531>3.3.CO;2-E](https://doi.org/10.1002/1522-2624(200010)163:5<531::AID-JPLN531>3.3.CO;2-E).
 772 Kern, J., Giani, L., Teixeira, W., Lanza, G., Glaser, B., 2019. What
 773 can we learn from ancient fertile anthropic soil (Amazonian
 774 Dark Earths, shell mounds, Plaggen soil) for soil carbon
 775 sequestration? *Catena*, 172, 104-112.
 776 <https://doi.org/10.1016/j.catena.2018.08.008>
 777 Kramer, M.G., Sollins, Ph., Sletten, R.S., Swart, P.K., 2003. N
 778 isotope fractionation and measures of organic matter alteration
 779 during decomposition. *Ecology* 84, 2021-2025.
 780 <https://doi.org/10.1890/02-3097>
 781 Leenheer, J.A., 1980. Origin and nature of the humic substances in
 782 the waters of the Amazon River basin. *Acta Amazonica* 10,
 783 513–526. <https://doi.org/10.1590/1809-43921980103513>
 784 Lucas, Y., Boulet, R., Veillon, L., 1987. Systèmes sols ferrallitiques -
 785 podzols en région amazonienne. In Righi, D., Chauvel, A.
 786 (Eds.), *Podzols et Podzolisation*. AFES, Plaisir and INRA, Paris,
 787 pp. 53-65.

788 Lucas, Y., Montes, C.R., Mounier, S., Loustau-Cazalet, D., Ishida,
 789 D., Achard, R., Garnier, C. Melfi, A.J., 2012. Biogeochemistry
 790 of an amazonian podzol-ferralsol soil system with white kaolin.
 791 Biogeoscience 9, 3705-3720. [https://doi.org/10.5194/bg-9-3705-](https://doi.org/10.5194/bg-9-3705-2012)
 792 2012
 793 Lucas Y., 2001. The role of the plants in controlling rates and
 794 products of weathering: importance of the biological pumping.
 795 Ann. Rev. Earth Planet. Sci. 29, 35-163.
 796 <https://doi.org/10.1146/annurev.earth.29.1.135>
 797 Lucas, Y., Nahon, D., Cornu, S., Eyrolle, F., 1996. Genèse et
 798 fonctionnement des sols en milieu équatorial. C . R. Acad. Sci.
 799 Paris Ser. IIA 322, 1-16. [http://horizon.documentation.ird.fr/exl-](http://horizon.documentation.ird.fr/exl-doc/pleins_textes/pleins_textes_6/b_fdi_43-44/010004553.pdf)
 800 [doc/pleins_textes/pleins_textes_6/b_fdi_43-44/010004553.pdf](http://horizon.documentation.ird.fr/exl-doc/pleins_textes/pleins_textes_6/b_fdi_43-44/010004553.pdf)
 801 Lucas Y., Santin R.C., Silva W.T.L. da, Merdy P., Melfi A.J., Pereira
 802 O.J.R., Montes C.R., 2020. Soil sample conservation from field
 803 to lab for heterotrophic respiration assessment. MethodsX 7,
 804 101039. <https://doi.org/10.1016/j.mex.2020.101039>
 805 Marques, J.D.D.O., Luizão, F.J., Teixeira, W.G., Vitel, C.M.,
 806 Marques, E.M.D.A., 2016. Soil organic carbon, carbon stock
 807 and their relationships to physical attributes under forest soils in
 808 central Amazonia. Revista árvore 40, 197-208.
 809 Marques, J.D.O., Luizão, F., Teixeira, W., Nogueira, E., Fearnside,
 810 P., Sarrazin, M., 2017. Soil carbon stocks under Amazonian
 811 forest: distribution in the soil fractions and vulnerability to
 812 emission. Open J. Forest. 7, 121-142.
 813 <https://doi.org/10.4236/ojf.2017.72008>.
 814 Merdy, P., Lucas, Y., Coulomb, B., Melfi, A.J., Montes, C.R., 2021.
 815 Soil organic carbon mobility in equatorial podzols: soil column

816 experiments. *Soil* 7, 585–594. <https://doi.org/10.5194/soil-7->
817 585-2021.

818 Miller, A.E., Schimel, J.P., Meixner, T., Sickman, J.O., Melack,
819 J.M., 2005. Episodic rewetting enhances carbon and nitrogen
820 release from chaparral soils. *Soil Biol Biochem.* 37, 2195–2204.
821 <https://doi.org/10.1016/j.soilbio.2005.03.021>

822 Milori, D.M.B.P., Martin-Neto, L., Bayer, C., Mielniczuk, J.,
823 Bagnato, V.S., 2002. Humification degree of soil humic acids
824 determined by fluorescence spectroscopy. *Soil Sci.* 167, 739-
825 749. <https://doi.org/10.1097/00010694-200211000-00004>

826 Milori, D.M.B.P., Galeti, H.V.A, Martin-Neto, L., Dieckow, J., Pérez,
827 M.G., Bayer, C., Salton, J., 2006. Organic matter study of whole
828 soil samples using laser-induced fluorescence spectroscopy. *Soil*
829 *Sci. Soc. Am. J.* 70, 57–63.
830 <https://doi.org/10.2136/sssaj2004.0270>

831 Montes, C.R., Lucas, Y., Pereira, O.J.R., Achard, R., Grimaldi, M.,
832 Melfi, A.J., 2011. Deep plant-derived carbon storage in
833 Amazonian podzols. *Biogeosciences* 8, 113-120.
834 <https://doi.org/10.5194/bg-8-113-2011>

835 Munsell, 1990. Munsell soil color chart, Kollmorgen Instruments
836 Corp., New York.

837 Paul, E.A., Morris, S.J., Bohm, S., 2001. The determination of soil C
838 pool sizes and turnover rates: biophysical fractionation and
839 tracers. In: Lal, R., Kimble, J.M., Follet, R.F., Stewart, B.A.
840 (Eds.), *Assessment Methods for Soil Carbon*, Lewis Publishes,
841 Boca Raton, pp. 193–206 .

842 Pereira, O.J.R., Montes, C.R., Lucas, Y., Santin, R.C., Melfi, A.J.,
843 2015. A multi-sensor approach for mapping plant-derived

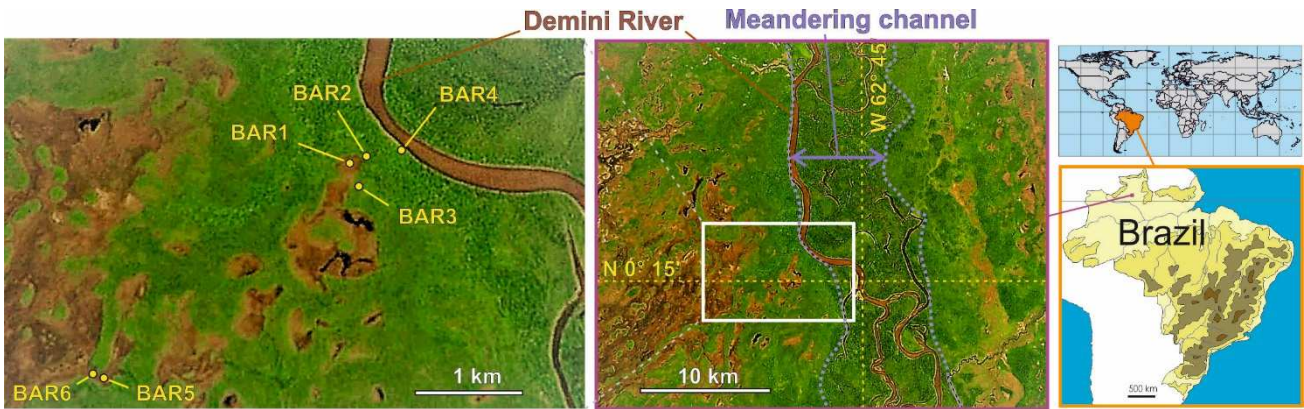
844 carbon storage in Amazonian podzols. *Int. J. Rem. Sens.* 36,
845 2076-2092. <http://dx.doi.org/10.1080/01431161.2015.1034896>
846 Pereira, O.J.R., Montes, C.R., Lucas, Y., Melfi, A.J., 2016.
847 Evaluation of pedotransfer equations to predict deep soil carbon
848 stock in tropical Podzols compared to other soils of Brazilian
849 Amazon forest. In: *Digital Soil Morphometrics*, A.E. Hartemink
850 and B. Minasny (eds.), Chap. 21 (pp. 331-349), Series: Progress
851 in Soil Science, Springer. [https://doi.org/10.1007/978-3-319-](https://doi.org/10.1007/978-3-319-28295-4_21)
852 [28295-4_21](https://doi.org/10.1007/978-3-319-28295-4_21)
853 Qiao, N., Xu, X., Hu, Y., Blagodatskaya, E., Liu, Y., Schaefer, D.,
854 Kuzyakov, Y., 2016. Carbon and nitrogen additions induce
855 distinct priming effects along an organic-matter decay
856 continuum. *Scientific Reports* 6, 1-8.
857 <https://doi.org/10.1038/srep19865>.
858 Reboita, M.S., Gan, M.A., Rocha, Rosmeri, P. da, Ambrizzi, T.,
859 2010. Regimes de precipitação na América do Sul: uma revisão
860 bibliográfica. *Rev. Bras. Meteorol.* 25, 185-204.
861 <https://dx.doi.org/10.1590/S0102-77862010000200004>
862 Reis, N.J., Almeida, M.E., Riker, S.L., Ferreira, A.L., 2006. *Geologia*
863 *e Recursos Minerais do Estado do Amazonas*. CPRM – Serviço
864 Geológico do Brasil, maps and notice, 125p.
865 Scheinost, A.C., Chavernas, A., Barrón, V., Torrent, J., 1998. Use
866 and limitations of second-derivative diffuse reflectance
867 spectroscopy in the visible to near-infrared range to identify and
868 quantify Fe oxide minerals in soils.
869 Sohi, S.P., Mahieu, N., Arah, J.R.M., Powlson, D.S., Madari, B.,
870 Gaunt, J.L., 2001. A procedure for isolating soil organic matter

871 fractions suitable for modeling. *Soil Sci. Soc. Am. J.* 65, 1121–
 872 1128. <https://doi.org/10.2136/sssaj2001.6541121x>
 873 Swift, R., 1996. Organic matter characterization. In: Sparks, D.L.,
 874 Page, A.L., Helmke, P.A., Loeppert, R.H., Soltanpour, P.N.,
 875 Tabatabai, M.A., Johnson, C.T., Sumner, M.E. (eds), *Methods*
 876 *of soil analysis, Part 3: chemical methods*. SSSA Book Series
 877 N°5, SSSA and ASA, Madison, WI, 1011–1069.
 878 <https://doi.org/10.2136/sssabookser5.3.c35>
 879 Tadini, A.M., Nicolodelli, G., Senesi, G.S., Ishida, D.A., Montes,
 880 C.R., Lucas, Y., Mounier, S., Guimarães, F.E.G., Milori,
 881 D.M.B.P., 2018. Soil organic matter in podzol horizons of the
 882 Amazon region: Humification, recalcitrance, and dating. *Sci.*
 883 *Tot. Environ.* 613-614, 160-167.
 884 <https://doi.org/10.1016/j.scitotenv.2017.09.068>
 885 Tardy, Y., Roquin, C., Bustillo, V., Moreira, M., Martinelli, L.A.,
 886 Victoria, R., 2009. Carbon and Water Cycles, Amazon River
 887 Basin, *Applied Biogeochemistry*. Atlantica, Biarritz.
 888 Trumbore, S., 2000. Age of soil organic matter and soil respiration:
 889 radiocarbon constraints on belowground C dynamics. *Ecol.*
 890 *Appl.* 10, 399-411. [https://doi.org/10.1890/1051-](https://doi.org/10.1890/1051-0761(2000)010[0399:AOSOMA]2.0.CO;2)
 891 [0761\(2000\)010\[0399:AOSOMA\]2.0.CO;2](https://doi.org/10.1890/1051-0761(2000)010[0399:AOSOMA]2.0.CO;2).
 892 Van Gestel, M., Merckx, R., Vlassak, K., 1993. Microbial biomass
 893 and activity in soils with fluctuating water contents. In *Soil*
 894 *Structure/Soil Biota Interrelationships*, Elsevier, pp. 617-626.
 895 <https://doi.org/10.1016/B978-0-444-81490-6.50050-9>.
 896 Wei, H., Chen, X., Xiao, G., Guenet, B., Vicca, S., Shen, W., 2015.
 897 Are variations in heterotrophic soil respiration related to changes
 898 in substrate availability and microbial biomass carbon in the

899 subtropical forests? Scientific Reports 5, 1-11.
900 <https://doi.org/10.1038/srep18370>.
901 Yang, L., Pan, J., Shao, Y., Chen, J. M., Ju, W. M., Shi, X., Yuan, S.,
902 2007. Soil organic carbon decomposition and carbon pools in
903 temperate and sub-tropical forests in China. J. Env. Manag. 85,
904 690-695. <https://doi.org/10.1016/j.jenvman.2006.09.011>

905 **Fig. 1**

906

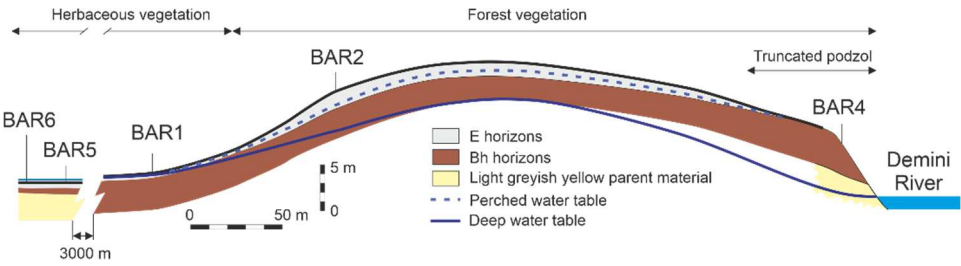


908

909

910 **Fig. 2**

911



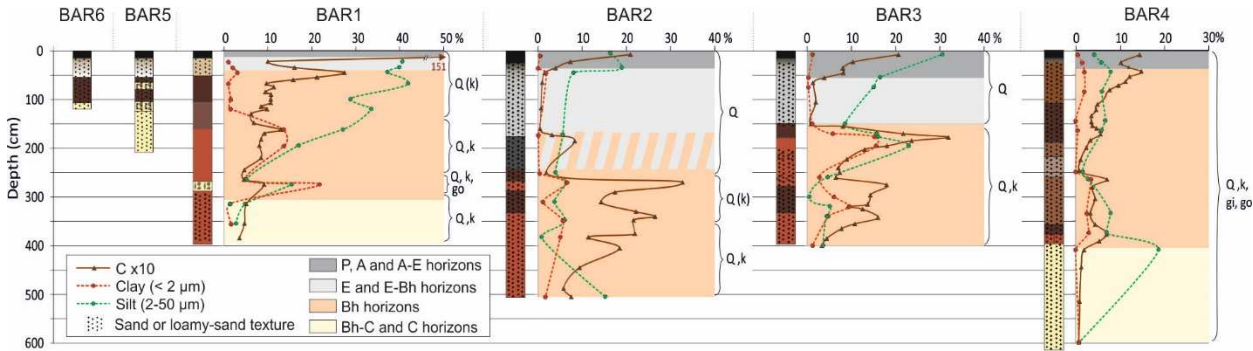
912

913

914

915 **Fig. 3**

916

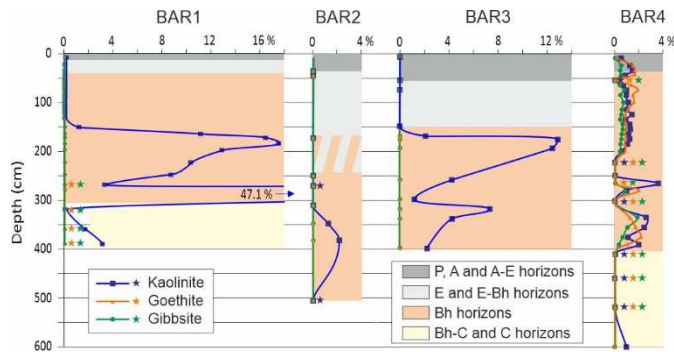


918

919

920 **Fig. 4**

921



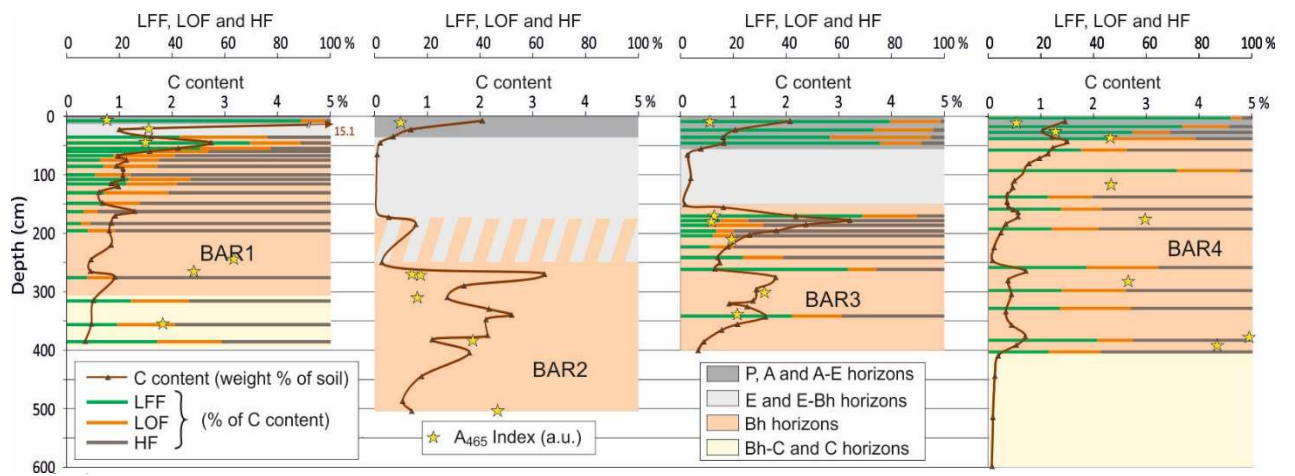
922

923

924

925 **Fig. 5**

926



928

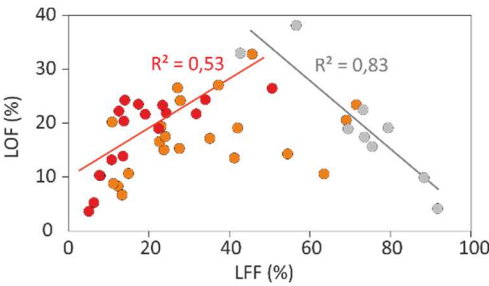
929

930

931

932 **Fig. 6**

933



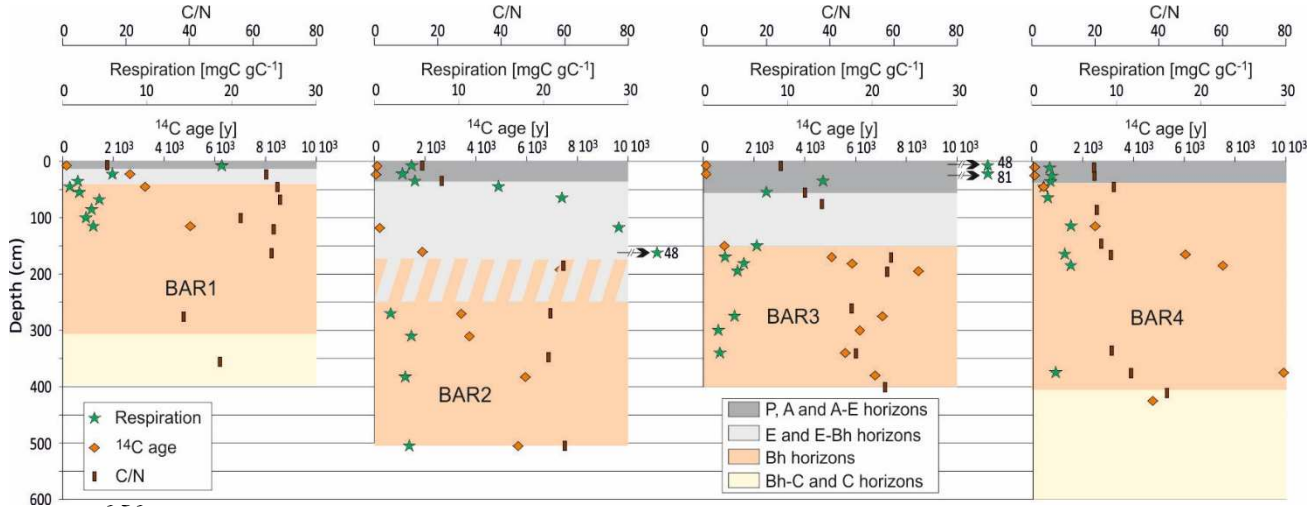
934

935

936

937 **Fig. 7**

938



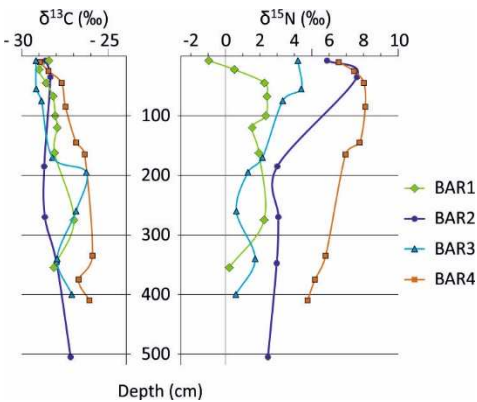
940

941

942

943 **Fig. 8**

944



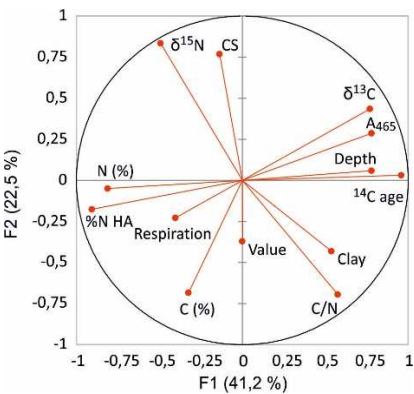
945

946

947

948 **Fig. 9**

949



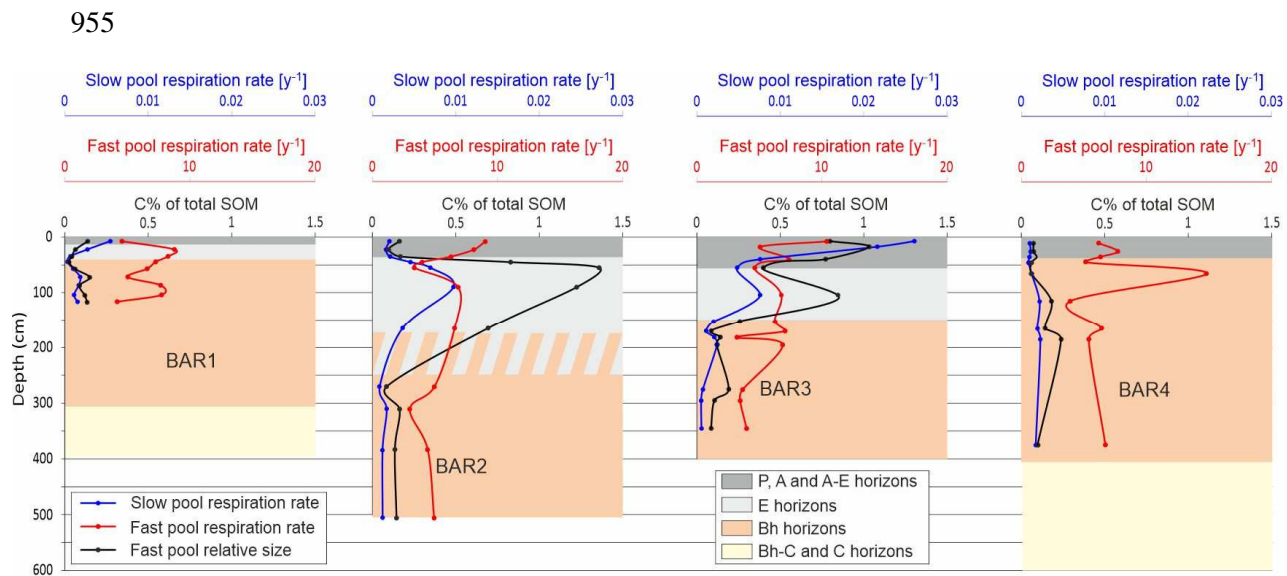
950

951

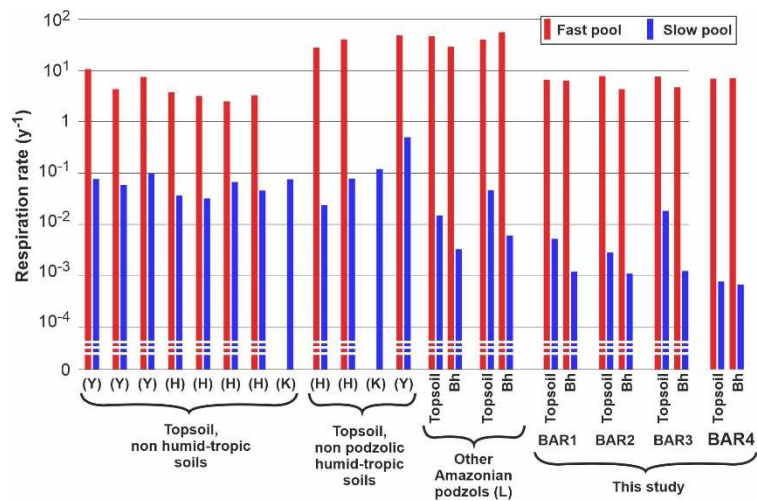
952

953

954 **Fig. 10**

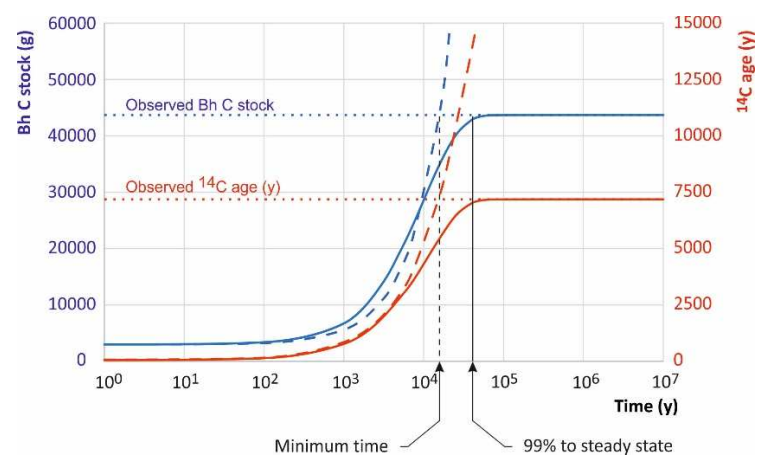


959 **Fig. 11**



964 **Fig. 12**

965



966

967

968

969 **Figure caption**

970

971 **Fig. 1.** Location of the studied site

972

973 **Fig. 2.** Situation of the soil profiles with regard to topography and
974 sketch of the horizon geometry.

975

976 **Fig. 3.** The studied profiles: borehole logs (colours seek to reflect
977 actual colours); C (carbon), clay and silt in %; mineralogy. Q: quartz,
978 k: kaolinite, gi: gibbsite, go: goethite (uppercase: dominant mineral;
979 lowercase in parentheses: trace mineral only). E-Bh horizons:
980 transition between E and Bh horizons; Bh-C horizons: transition
981 between Bh and C horizons.

982

983 **Fig. 4.** Quantifiable kaolinite, goethite and gibbsite in the BAR1
984 to BAR4 profiles. A star indicates that the given mineral has been
985 identified but in a quantity too small to be quantified.

986

987 **Fig. 5.** Organic matter fractionation and A_{465} humification index.
988 LFF: light free fraction, LOF: light occluded fraction, HF: heavy
989 fraction.

990

991 **Fig. 6.** Relationships between LFF and LOF % in SOM. Grey
992 points: P, A and A-E horizons; red and orange points: Bh and B-C
993 horizons. Red points refer to the BAR1 profile.

994

995 **Fig. 7.** SOM apparent ^{14}C age, C/N values and cumulative
996 respiration at 660 days.

997

998 **Fig. 8.** SOM isotopic data

999

1000 **Fig. 9.** PCA correlation circles on the first two factorial axes.

1001 Percent on each factorial axis gives the explained variance. Value:

1002 value of the horizon Munsell color; %N HA: % of N in the extracted

1003 humic acid fraction of the SOM (data from Tadini et al., 2018). CS:

1004 coarse sand.

1005

1006 **Fig. 10.** Relative size of the SOM fast pool (C% of the total SOM)

1007 and respiration rates of the slow and fast pool.

1008

1009 **Fig. 11.** Respiration rates of fast and slow pools of soil organic

1010 matter. (Y): Yang et al., 2007; (H): Haddix et al., 2011; (K) : Kern et

1011 al., 2019 ; (L): Lucas et al., 2020.

1012

1013 **Fig. 12.** Modelling the time of genesis. Dashed lines: scenario for

1014 minimum time; plain lines: scenario for steady state.

1015

